Docking Essential Dynamics Eigenstructures

Diana Mustard and David W. Ritchie*

[dmustard,dritchie]@csd.abdn.ac.uk

Department of Computing Science,
University of Aberdeen,
Aberdeen AB24 3UE,
Scotland, U.K.
Tel. (+44)(–0)1224 272282
Fax (+44)(–0)1224 273422

* Corresponding author

Abstract

This article describes our attempts to dock the targets in CAPRI Rounds 3–5 using *Hex* 4.2, and it introduces a novel essential dynamics approach to generate multiple feasible conformations for docking. In the blind trial, the basic *Hex* algorithm found one high accuracy solution for CAPRI target 12, and several further medium and low accuracy solutions for targets 11, 12, 13, and 14. Subsequent *a posteriori* docking of the targets using essential dynamics "eigenstructures" was found to give consistently better predictions than rigidly docking only the unbound or model-built starting structures. Some suggestions to improve this promising new approach are presented.

Key words

Hex; CAPRI; protein docking; distance constraints; essential dynamics; eigenvector analysis; eigenstructures; polar Fourier correlation

Introduction

Protein-protein docking algorithms aim to predict how a pair of proteins might bind or "dock" using knowledge only of the three-dimensional (3D) structures of the separate components. Most current algorithms assume the proteins to be docked are rigid. Any conformational changes on going from the unbound to the bound protein structures are then typically absorbed or ignored by using "soft" scoring functions (for a review, see e.g. [1]). However, the rigid body assumption is often an unrealistic idealisation which can cause many false-positive predictions. One way to reduce the number of false-positives is to use biochemical knowledge to filter the solutions [2]. Alternatively, protein flexibility may be simulated using molecular dynamics (MD) [3] or by docking multiple conformations from MD snapshots [4]. Recently, a principal component analysis of MD trajectories was used to accelerate flexible protein-ligand docking calculations [5]. However, MD-based approaches remain computationally expensive because long time-scale simulations are required to explore fully each protein's conformational space. Hence there is a need to develop more efficient ways of modelling protein flexibility during docking.

This article describes our attempts to dock the targets in CAPRI Rounds 3–5 (targets T8–T14, T18, T19) using *Hex* 4.2 [6, 7]. It also introduces current work towards developing an efficient way to model protein conformational change during docking. This novel approach uses an adaptation of the Distance Constraint Essential Dynamics (DCED) technique [8, 9] to generate multiple feasible conformations for docking, which we call "eigenstructures." Because this work is on-going, the results reported for docking DCED eigenstructures were obtained retrospectively, after the coordinates of the CAPRI target complexes had been made available. Overall, the basic *Hex* approach found one high accuracy solution for target 12 (T12), and several further medium and low accuracy solutions for targets 11, 12, 13, and 14. In all cases, the retrospective DCED docking results show a moderate but consistent improvement when docking multiple eigenstructures compared to docking only the unbound or model-built starting structures. This indicates further development of the approach would be worthwhile.

Methods

Target Preparation

For the majority of the targets, the docking predictions submitted to CAPRI were made using shape-only *Hex* correlations to order N=30. Because the unbound structures of several of the targets were given as homologues, Modeller 4.0 [10] with default parameters was used as necessary to build a model from the template recommended by the CAPRI organisers. We used available evidence from the literature to try to identify or predict the location of one or both epitopes for each target. For example, for T8, laminin is reported to bind to nidogen via the $\gamma 4$ domain [11]. Hence the $\gamma 4$ loop was manually oriented to face the main propeller axis of nidogen, and one angular search constraint [6] was used to keep it towards the nidogen during docking. T9 (LiCT homodimer) was modelled from the unphosphorylated structure, PDB code 1H99. We presumed there would be relatively little conformational change on phosphorylation, and hence set tight search constraints to permit only small rotational/translational movements from the orientation of the unphosphorylated homodimer.

Predicting the structure for the trimeric TBEV envelope protein was an interesting challenge. As suggested by the CAPRI organisers, we assumed the complex would have trimeric symmetry and focused the search around the membrane-distal domain II. Initially, three monomers (A, B, C) were superposed and centred at the origin. Keeping molecule A fixed, a pairwise A-B docking search was performed and for every rigid body transformation T applied to molecule B, molecule C was transformed by T^{-1}. A distance filter was then applied to eliminate orientations in which the A-B, A-C, and B-C distances between the domain II centroids differed by more than 3Å. This gave a small ranked list of surviving orientations, of which visual inspection found just two with near perfect three-fold symmetry. These were submitted as our predictions for this target.

The cohesin/dockerin complex presented another interesting target (T11, T12). There is stochiometric evidence that when dockerin binds to cohesin it disrupts the cohesin

domain dimer [12]. We therefore supposed that there would be a surface patch on dockerin that mimics part of the cohesin surface buried in the dimer. Hence we used *Hex*'s surface skin shape similarity correlation mode to superpose dockerin onto the B domain of the cohesin A-B dimer (PDB code 1AOH) in order to give a starting orientation for docking with both presumed binding sites initially in contact. The rank-4 superposition was selected as the starting orientation because this was seen to bring into contact many of the residues that had been implicated as key binding residues in previous studies [12, 13]. This approach was used for both T11 (docking an NMR dockerin homologue) and T12 (dockerin coordinates provided from the crystal structure of the complex).

For T13 (antibody-SAG1), we presumed that the antibody would bind to the SAG1 N-terminal D1 domain because the C-terminal domain of SAG1 is attached as a dimer to the *Toxoplasma gondii* cell surface [14]. Hence the A-chain D1 domain was initially positioned close to the antibody hypervariable loops, and angular constraints were used to limit the correlation to the hypervariable region. Docking was performed in the presence of the B chain in order to "block" the distal surface of the A-chain D1 domain. Prior structural knowledge was also available for T14 (PP1-MYPT1). The KVKF motif residues 35-38 of MYPT1 which are known to play a key role in binding PP1c [15] were manually located in the PP1 hydrophobic binding groove identified by Egloff *et al.* [16] in such a way as to avoid as far as possible producing steric clashes between the rest of the two structures. For T18 (xylanase-TAXI), we restricted the docking search to the xylanase catalytic site [17] and sampled all parts of the TAXI surface during the docking run. Because the TAXI structure was provided in its bound form yet still contained unresolved surface loops, any docking orientations that contained these loop regions were manually rejected on the assumption that all binding site residues would be fully resolved in the complex. For T19 (prion-Fab), the prion protein was modelled from the recommended template (PDB code 1DWY). The docking search was constrained to the antibody hypervariable loop regions, but ranged over the whole prion surface.

Generating DCED Eigenstructures

We use the CONCOORD and DISCO programs [9] to generate a large number of pseudo-random 3D protein conformations. This ensemble of structures may be considered as permissible sample points within the multi-dimensional conformational space of the protein. In order to capture the most significant fluctuations within this space, the essential dynamics (ED) approach constructs a square covariance matrix $\underline{C}$ of the means of the deviations of each atom's coordinates x_i from its average (or in this work, its *initial unbound*) position u_i:

$$C_{ij} = <(x_i - u_i)(x_j - u_j)>, \tag{1}$$

where the subscripts $i, j = 1...3N$ label the components of the Cartesian coordinates of the N atoms under consideration. Hence a least $3N$ conformational samples are required for an ED analysis. The covariance matrix may be diagonalised to solve for $\underline{T}$ and $\underline{\Lambda}$:

$$\underline{C} = \underline{T}.\underline{\Lambda}.\underline{T}^T \tag{2}$$

where $\underline{T}$ is the matrix of eigenvectors, $\underline{e}_k$, and $\underline{\Lambda}$ is a diagonal matrix of eigenvalues, λ_k. The eigenvectors and eigenvalues represent the principal components and squared magnitudes of the coordinate fluctuations in $\underline{C}$, respectively. If the eigenvectors are considered in order of decreasing size of their corresponding eigenvalues, most of the fluctuation is found within in the first few eigenvectors. Hence the DCED technique captures much of the internal motion of a protein whilst avoiding most of the computational expense of running a full MD simulation [8].

Here, we adapt the above approach to generate feasible starting structures for docking by first performing a DCED analysis on the initial conformation of the starting structure. Because the eigenvectors are orthonormal and span the conformational coordinate space of the protein, any 3D conformation may, in principle, be constructed from an appropriate combination of eigenvectors. For example, denoting vectors of bound and unbound protein coordinates by $\underline{B}$ and $\underline{U}$ (with $\underline{U} = \{u_i; i = 1...3N\}$, etc.), we may write

$$\underline{B} = \underline{U} + \sum_k \alpha_k \underline{e}_k. \tag{3}$$

The coefficients α_k represent the weights with which the eigenvectors should be combined in order to obtain the bound conformation from the coordinates of the unbound structure. When the unbound and bound coordinates are known, we call the quantity

$$\underline{V} = \underline{B} - \underline{U} \tag{4}$$

the "docking vector," and the weights α_k may be solved exactly using a projection:

$$\alpha_k = \underline{V}.\underline{e}_k. \tag{5}$$

This provides a useful way to evaluate the approach with known complexes. Figure 1 shows the C_α RMS deviation between the calculated and actual bound conformations as a function of the number of eigenvectors used in Eq 3. This shows that the first few eigenvectors can account for much of the backbone conformational change that takes place on binding. Of course, in predictive docking the desired bound conformation is unavailable, and indeed the initial unbound conformation may have been model-built. Nonetheless, we assume that following an ED analysis of the starting structure, there will exist some combination of the most significant eigenvectors which will transform it into one that resembles more the bound form. In other words, we assume that each conformation is accessible from the other through the fluctuation modes embedded in its structure. The task then reduces to calculating the weights with which a sufficient number of eigenvectors should be combined.

[Figure 1 about here.]

In our approach, the DCED analysis is applied to the heavy atoms C_α, C, O, N, and C_β (if present). Then, each candidate backbone conformation $\underline{B}_{nj}$ is constructed as:

$$\underline{B}_{nj} = \underline{U} + \sum_{k=1}^{n} \alpha_{kj}\underline{e}_k \tag{6}$$

where the subscript j enumerates samples along the kth eigenvector, $\alpha_{kj} = \pm\delta, \pm2\delta$, etc. We typically use $\delta = 0.25$Å. Thus each candidate conformation deviates from all others by an integral multiple of 0.25Å RMS. However, many of these conformations will have

infeasible covalent bond lengths and angles. Hence, we arbitrarily define any covalent bond which differs by more than 1% from the original structure as a "bad bond," and we reject any conformation with more than five bad bonds. In our current implementation, up to $n=8$ eigenvectors are sampled while $|\alpha_{kj}| \leq \sqrt{\lambda_k}$, which can produce up to around 10^5 candidate backbone conformations. Applying our simple bond length filter typically reduces this number to less than 100. Because these candidate structures have locally very similar backbone geometries to the starting conformation, side chain atom coordinates are transferred directly from the starting structure. We call the resulting 3D protein structures "eigenstructures." In the current study, eigenstructures were generated for just one of the proteins in each complex (typically the unbound or smaller component, which we consider as the "ligand"), primarily to avoid the computational expense of multiple cross-dockings.

Table I summarises the number of conformational models generated and filtered for the CAPRI targets using the above procedure (this table omits the very flexible T9 LiCT structure; T18 is also omitted because the TAXI ligand does not have a contiguous backbone, as required by CONCOORD). The final three columns of RMS deviations show that in all cases conformations can be generated which have a lower C_α deviation from the bound form than the initial unbound structure. For example, when using a projection on the first eight eigenvectors, the unbound-bound C_α deviation for T8 is reduced by 0.58Å RMS from 1.88 to 1.30Å RMS. For T17, the corresponding reduction is 0.70Å RMS. With blind eigenvector sampling using a fixed step size, the reduction available in the RMS deviations is less than the above theoretical optimum, but it can still be significant in favourable cases (e.g. 0.26 and 0.21Å RMS, for T8 and T17, respectively). Hence, Table I shows that improved backbone conformations may be generated with relatively little effort in the DCED approach.

[Table I about here.]

7

Results

The CAPRI Docking Predictions

Using the assessment criteria of Mendez & Wodak described in this issue [18], the best *Hex* predictions were made for the cohesin/dockerin targets [19], with one high and two low accuracy solutions for target T12 (docking the dockerin X-ray structure; dockerin RMSD 1.87Å), and with one medium and two low accuracy solutions for T11 (docking the NMR dockerin homologue). *Hex* also found one low accuracy solution for T13, and three low accuracy solutions for T14 [20]. Two plausible trimeric complexes were produced for T10. Although the predicted contact surfaces largely involved the TBEV domain-II monomers, they did not exhibit the more extended domain contacts present in the revealed crystal structure [21]. We presume this is because we assumed the monomer to be rigid, when in fact extensive inter-domain motion occurs on assembly of the trimer [21]. Despite using considerable prior knowledge from the literature as summarised above, *Hex* failed to find good predictions for the remaining targets. We ascribe this to the large conformational changes observed in T8 and T9, and to the additional difficulty of docking model-built structures, e.g. T19.

Docking DCED Eigenstructures

In order to investigate the utility of our eigenstructure docking approach, we retrospectively docked ED-generated eigenstructures for those targets amenable to DCED analysis. Because by this stage the crystal structures of the complexes had been revealed, we chose to start each docking run with the eigenstructures initially superposed onto the C_α atoms of the complex. All docking runs in this test used shape-only N=30 correlation and 45 degree angular search constraints on each protein. In some cases, the eigenvector step size and bond length filter parameters were modified slightly (e.g. for T8 and T14) in order to achieve a more manageable list of eigenstructures (< 100) to be docked. Each list of eigenstructures was then seeded with the conformations of the unbound and bound ligand

structures in order to permit a direct comparison of docking the three types of structure. Due to the large number of orientational samples generated, all docking solutions were sorted and clustered as described previously [7]. The total computational cost was around 12 CPU-hours per complex on a 1.8GHz AMD Athlon processor.

Table II summarises the results of this test. For example, the first low RMS orientation found for T8 is the eigenstructure which appears as the first member (out of 94) of the 30th cluster. This orientation has a lower RMS deviation from the complex than the initial unbound conformation, which appears at position 40 in the same cluster. The bound conformation appears further down the list in cluster 84 (at position 1 of 2). Thus our scoring function ranks the bound conformation less favourably than the other two structures. Similar trends are seen for the remaining complexes. Contrary to previous rigid-body results [6], the bound conformation is ranked less favourably than the unbound one in several cases. We believe this is due to the very large number of decoy conformations in the docking list. On the other hand, considering the clusters containing the unbound structures, in almost all cases the scoring function places a comparable or lower RMS eigenstructure at a better rank than the unbound conformation. This indicates that the DCED approach is successfully generating improved trial docking conformations compared to docking the initial unbound or model-built structures.

[Table II about here.]

Discussion

Overall, the blind predictions made by *Hex* were fairly successful, with one high accuracy prediction for T12, and with several further medium and low accuracy predictions for targets 11, 12, 13, and 14. The novel superposition approach used to set up the cohesin/dockerin docking runs (see Methods) was useful in helping to identify our good prediction for the challenging case of T11 (docking the NMR dockerin homologue). Similarly for T13 and T14, prior knowledge of the binding site(s) was sufficient to help *Hex* find

several reasonably acceptable solutions. On the other hand, *Hex* failed to find good solutions for the remaining targets despite the use of considerable prior knowledge from the literature. The difficulty in these cases was largely due to the conformational changes that occur on binding, or conformational inaccuracies in our model-built starting structures.

Our initial studies on DCED eigenstructures seem very promising. We have shown that the first few eigenvectors intrinsically encode much of the backbone conformational flexibility observed on binding. The results with the CAPRI targets show that docking multiple eigenstructures generated from the first eight eigenvectors is sufficient to give better docking predictions than docking only the initial unbound or model-built structures. However, there is clearly scope to improve the quality of the generated conformations. For example, increasing the number of eigenvectors sampled and using a variable step size to search along each eigenvector should give better coverage of the conformational space accessible to each protein. Additionally, using a more sensitive method of estimating and possibly minimising the internal energies of the generated eigenstructures should give more physically realistic structures within that space. However, it will also be necessary to make the docking scoring function more selective in order to identify a near-native conformation of the complex from a large repertoire of physically realistic decoys.

Conclusion

The results obtained for the CAPRI targets using *Hex* show that in favourable cases useful rigid-body predictions can be made for relatively difficult protein-protein docking problems, particularly when some prior knowledge of the system is available. However, there is clearly a need to develop better ways of modelling protein flexibility during docking. Our initial results obtained from docking DCED eigenstructures indicate that this new approach presents a promising and tractable way to address this problem, and that further development of the technique would be both worthwhile and feasible.

Acknowledgments

References

1. I. Halperin, B. Ma, H. Wolfson, and R. Nussinov. Principles of docking: An overview of search algorithms and a guide to scoring functions. *Proteins: Struct. Func. Genet.*, 47:409–443, 2002.

2. H. A. Gabb, R. M. Jackson, and M. J. E. Sternberg. Modelling protein docking using shape complementarity, electrostatics and biochemical information. *J. Mol. Biol.*, 272(1):106–120, 1997.

3. T. Wang and R. C. Wade. Implicit solvent models for flexible protein-protein docking by molecular dynamics simulation. *Proteins: Struct. Func. Genet.*, 50:158–169, 2003.

4. R. Grünberg, J. Leckner, and M. Nilges. Complementarity of structure ensembles in protein-protein docking. *Structure*, 12:2125–2136, 2004.

5. M. Zacharias. Rapid protein-ligand docking using soft modes from molecular dynamics simulations to account for protein deformability: binding of FK506 to FKBP. *Proteins: Struct. Func. Bioinf.*, 54:759–767, 2004.

6. D. W. Ritchie and G. J. L. Kemp. Protein docking using spherical polar Fourier correlations. *Proteins: Struct. Func. Genet.*, 39(2):178–194, 2000.

7. D. W. Ritchie. Evaluation of protein docking predictions using *Hex* 3.1 in CAPRI rounds 1 and 2. *Proteins: Struct. Func. Genet.*, 52(1):98–106, 2003.

8. A. Amadei, A. B. M. Linssen, and H. J. C. Berendsen. Essential dynamics of proteins. *Proteins: Struct. Func. Genet.*, 17:412–425, 1993.

9. B. L. de Groot, D. M. F. van Aalten, R. M. Scheek, A. Amadei, G. Vriend, and H. J. C. Berendsen. Prediction of protein conformational freedom from distance constraints. *Proteins: Struct. Func. Genet.*, 29:240–251, 1997.

10. A. Šali and T. L. Blundell. Comparative protein modelling by satisfaction of spatial constraints. *J. Mol. Biol.*, 234:779–815, 1993.

11. U. Mayer, R. Nischt, E. Poschl, K. Mann, K. Fukuda, M. Gerl, Y. Yamada, and R. Timpl. A single EGF-like motif of laminin is responsible for high affinity nidogen binding. *EMBO J.*, 12:1879–1885, 1993.

12. S. Spinelli, H.-P. Fiérobe, A. Belaïch, J.-P. Belaïch, B. Henrissat, and C. Cambillou. Crystal structure of a cohesin module from *clostridium cellulolyticum*: Implications for dockerin recognition. *J. Mol. Biol.*, 304:189–200, 2000.

13. B. Lytle, B. F. Volkman, W. M. Westler, M. P. Heckman, and J. H. D. Wu. Solution of a type I dockerin domain, a novel prokaryotic, extracellular calcium-binding domain. *J. Mol. Biol.*, 307:745–753, 2001.

14. X.-L. He, M. E. Grigg, J. C. Boothroyd, and K. C. Garcia. Structure of the immunodominant surface antigen from the *toxoplasma gondii* SRS superfamily. *Nature Struct. Biol.*, 9:606–611, 2002.

15. D. J. Hartshorne. Myosin phosphatase: subunits and interactions. *Acta Physiol. Scand.*, 164:483–493, 1998.

16. M.-P. Egloff, D. F. Johnson, G. Moorhead, P. t. W. Cohen, P. Cohen, and D. Barford. Structural basis for the recognition of regulatory subunits by the catalytic subunit of protein phosphatase 1. *EMBO J.*, 16:1876–1887, 1997.

17. K. Gebruers, K. Brijs, C. M. Courtin, K. Fierens, H. Goesaert, A. Rabijns, G. Raedschelders, J. Robben, S. Sansen, J. F. Sorensen, S. Van Campenhout, and J. A. Delcour. Properties of TAXI-type endoxylanase inhibitors. *Biochim. Biophys. Acta*, 1696:213–221, 2004.

18. R. Méndez and S. J. Wodak. Protein-protein docking procedures are on the move. *Proteins: Struct. Func. Genet.*, 00:00–00, 2005.

19. A. L. Carvalho, F. M. V. Dias, J. A. M. Prates, T. Nagy, H. J.Gilbert, G. J. Davies, L. M. A. Ferreira, M. J. Romanao, and C. M. G. A. Fontes. Cellusome assembly revealed by the crystal structure of the cohesin-dockerin complex. *Proc. Natl. Acad. Sci.*, 13:552–557, 2003.

20. M. Terrak, F. Kerff, K. Langsetmo, T. Tao, and R. Dominguez. Structural basis of protein phosphatase 1 regulation. *Nature*, 429:780–784, 2004.

21. S. Bressanelli, K. Stiasny, S. L. Allison, E. A. Stura, S. Duquerroy, J. Lescar, F. X. Heinz, and F. A. Rey. Structure of a flavivirus envelope glycoprotein in its low-pH-induced membrane fusion conformation. *EMBO J.*, 23:728–738, 2004.
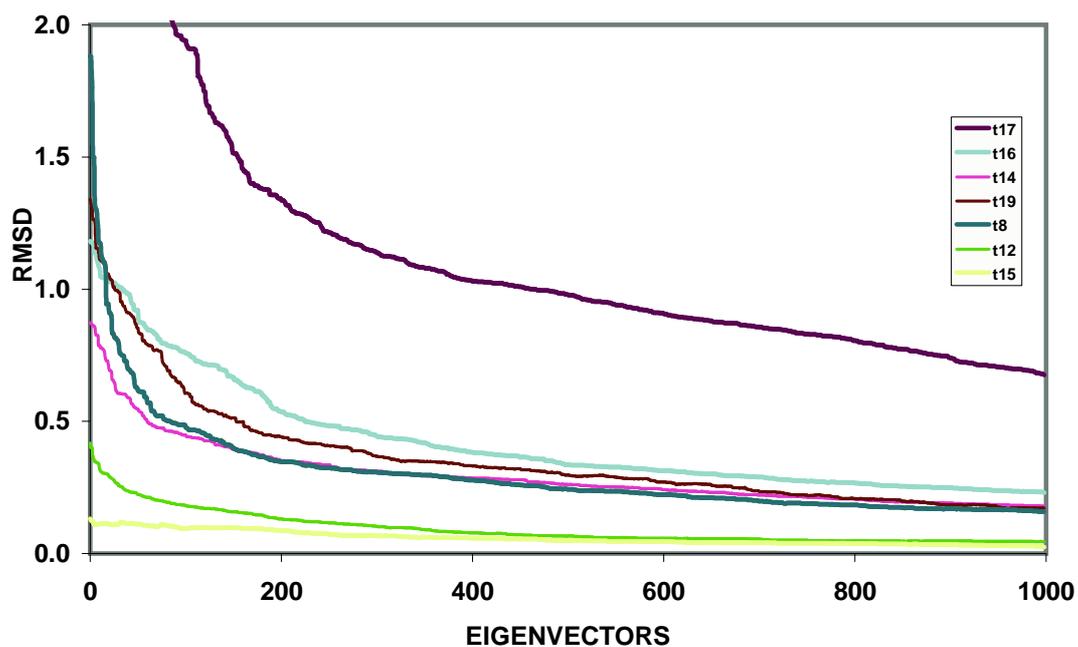
Figure 1: RMS deviation between the calculated and actual bound conformations of the CAPRI ligand structures as a function of the number of eigenvectors used in Eq 3. Eigenvectors are combined using weights α_k calculated from a projection (Eq 5) of the unbound-bound docking vector (Eq 4). The plots show that most of the conformational change that occurs on binding may be accounted for by the first few eigenvectors.

Table I: Eigenstructure Model Summary

Target	Ligand	AA[a]	EV[b]	CS[c]	ES[d]	B/UB[e]	B/ES(opt)[f]	B/ES(δ)[g]
T8	Laminin	162	8	405,405	624	1.88	1.30	1.62
T10	TBEV-B	395	6	8,505	49	11.33	10.90	11.13
T12	Dockerin	138	5	1,215	19	0.44	0.37	0.42
T13	SAG1	129	8	54,675	52	0.96	0.92	0.94
T14	PP1	294	8	59,535	229	0.88	0.83	0.85
T15	ImmD	87	5	2,025	6	0.15	0.11	0.15
T16	GH10	257	8	120,285	49	1.19	1.12	1.16
T17	GH11	188	8	54,675	33	5.09	4.39	4.88
T19	PrP	121	7	28,431	54	1.59	1.26	1.47

[a]The number of amino acids (AA) in the ligand structure.

[b]The number of eigenvectors (EV) used.

[c]The number of candidate structures (CS) generated from the eigenvectors using a step size of $\delta = 0.275$Å.

[d]The number of eigenstructures (ES) remaining after applying the bond length filter.

[e]The C_α RMS deviation between the bound and unbound structures.

[f]The best possible RMS deviation between the bound conformation and the optimal eigenstructure calculated from projections of the first 8 eigenvectors.

[g]The lowest C_α RMS deviation between the bound conformation and the best eigenstructure found when using a fixed step size (δ) search along the first 8 eigenvectors.

Table II: Eigenstructure Docking Summary[a]

Target	Docked ES	Bound	RMS	Unbound	RMS	ES	RMS
T8	94	84(1/2)	9.71	30(40/94)	8.80	30(1/94)	8.24
T11	37	19(1/5)	5.52	2(29/183)	9.55	2(1/183)	9.20
T12	40	1(1/90)	0.64	1(23/90)	1.53	1(6/90)	1.53
T13	52	5(1/9)	1.17	1(32/306)	0.96	1(1/306)	6.24
T14	60	16(1/3)	9.95	10(10/177)	8.81	10(1/177)	8.81
T15	39	20(6/17)	7.80	8(20/77)	3.47	8(1/77)	4.94
T17	33	3(1/8)	1.56	NF	NF	12(1/43)	8.64
T19	40	1(1/12)	0.95	13(46/66)	7.70	13(1/66)	5.28

[a]Listed are the number of ligand eigenstructures docked for each target followed by the cluster rank of the first solution with a C_α deviation of 10Å RMS or less obtained when docking bound, unbound, and DCED-generated eigenstructures, respectively. Figures in brackets (n/m) give the rank of the orientation (n) within the cluster of given size (m). NF denotes no low RMS solution found within the first 512 clusters.